RSC Advances

PAPER

View Article Online
View Journal | View Issue

Cite this: *RSC Adv.*, 2022, **12**, 35396

Preparation of ecofriendly water-borne polyurethane elastomer with mechanical robustness and self-healable ability based on multi-dynamic interactions†

Qingsong Shi,‡[a] Weilin Wu,‡[b] Bing Yu,[c] Mengqing Ren,[a] Lili Wu *[a] and Chaocan Zhang[a]

Self-healing materials have attracted widespread attention owing to their capacity to extend the lifetime of materials and improve resource utilization. However, achieving superior mechanical performance and high self-healable capability simultaneously under moderate conditions remains a long-standing challenge. Integrating multiple dynamic interactions in waterborne polyurethane (WPU) systems can overcome the above-mentioned issue. Herein, environmentally friendly WPU systems containing multiple hydrogen bonds and boronic ester bonds in their polymer backbones were synthesized, where 2,6-diaminopyridine (DAP) and boric acid (BA) served as a dynamic chain extender and reversible cross-linking agent, respectively. The chain structure of the polymer was adjusted by controlling the ratio (DAP/BA) of hard segments, which could effectively meet the requirement of mechanical robustness and desirable self-healable efficiency. Benefiting from multiple dynamic interactions, the prepared WPU elastomer exhibited good mechanical properties, such as tensile strength (from 18.89 MPa to 30.78 MPa), elongation (about 900%) and toughness (from 54.82 MJ m^{-3} to 92.74 MJ m^{-3}). Driven by water and heat, the IP-DAP_{40}-BA_{10}-WPU film cut in the middle exhibited good self-healing ability, with healing efficiencies of tensile stress of 90.74% and elongation of 91.29% after self-healing at 80 °C for 36 h. Meanwhile, the synthesized WPU elastomer exhibited good water resistance and thermal stability. This work presents a novel way to design robust self-healable materials, which will have wide promising applications in flexible electronics, smart coatings and adhesives.

Received 4th November 2022
Accepted 29th November 2022

DOI: 10.1039/d2ra07000f

rsc.li/rsc-advances

1 Introduction

Self-healable polymers are materials that can repair their mechanical damage either autonomously or under specific stimuli,[1] endowing these materials with self-healing ability, which can not only significantly improve their safety, stability and extend their lifetime but can also effectively reduce resource wastage and maintenance costs.[1–3] In recent years, self-healing polymer materials as primary media have shown considerable application prospects in flexible electronics and wearable devices, such as flexible electronic skin, intelligent coatings and durable sensors.[4–8] The polyurethane elastomer matrix with good flexibility and abrasion resistance, which can appropriately satisfy the robustness requirement, has attracted wide attention in scientific and engineering circles.[9,10]

Healable materials can be divided into intrinsic and extrinsic self-healable materials according to their healing mechanism.[1,11] A typical characteristic of extrinsic self-healable polymers is releasing the healing agent embedded in them to complete damage repair.[12–14] However, their preparation process is usually complicated and their low healing efficiency severely hinders their further development.[5] By contrast, intrinsic self-healable polymers mainly rely on the interactions of dynamic covalent bonds or noncovalent bonds in the polymer backbone. Dynamic covalent bonds mostly include urea bonds,[15,16] Diels–Alder bonds,[11,17] boronic ester,[12,18–21] disulfide bonds,[22–24] diselenide bonds[25] and phenol–carbamate bonds.[26] Noncovalent interactions include hydrogen bonds,[27–32] metal–ligand coordination,[33–37] ionic interactions,[38,39] host–guest interactions,[40] and π–π stacking interactions.[41,42] However, healing *via* DA ring addition and phenol–carbamate bonds requires high temperatures of up to 120 °C, which consumes a lot of energy.[43] Meanwhile, self-healing PU embedded with dynamic metal-coordinated bonds can heal at room

[a]*School of Materials Science and Engineering, Wuhan University of Technology, Wuhan 430070, P. R. China. E-mail: polym_wl@whut.edu.cn*

[b]*School of Pharmaceutical Sciences, Hunan University of Medicine, No. 492 South Jinxi Road, Huaihua, Hunan 418000, P. R. China*

[c]*MEGA P&C Advanced Materials (Shanghai) Co., Ltd., P. R. China*

† Electronic supplementary information (ESI) available. See DOI: https://doi.org/10.1039/d2ra07000f

‡ Qingsong Shi and Weilin Wu contributed equally to this work.

temperature, but this usually takes a long time and affords poor mechanical properties. Bao *et al.*[44] prepared polyurethanes with dynamic metal–ligand coordination and hydrogen bonds simultaneously, which exhibited high a healing efficiency of 98% and healed at ambient temperature for two days, but its tensile strength was 1.8 MPa. Zhang *et al.*[5] prepared polyurethanes with dynamic Cu–DOU coordination and hydrogen bonds for healing under ambient conditions, which exhibited excellent toughness (87 MJ m^{-3}), but healing took about six days, limiting its practical application. At present, the research hot spot is how to overcome the conflict in mechanical performance and self-healing efficiency, striving to obtain elastomer materials with outstanding mechanical properties and desirable self-healing ability under mild conditions.

Particularly, hydrogen bonds play a significant role in constructing self-healable polyurethanes because of their directivity and reversibility. Recently, Xia *et al.*[45] introduced hierarchical H-bonds in novel self-healable polyurethane backbones, which possessed high tensile stress (34.1 MPa) and superior toughness (127.3 MJ m^{-3}). Boric acids can form diverse reversible covalent and noncovalent bonds, and thus widely employed to construct self-healing polymer materials. The orientation of boric acid and boronic ester/boric acid can be adjusted easily by heating, adding water or Lewis base.[46,47] For example, Kai *et al.*[12] incorporated reversible boronic ester bonds, hydrogen bonds and B–N coordination in polyurethane healed at ambient temperature, which exhibited excellent tensile stress of 10.5 MPa and superior stretchability of 3120%. Previous researchers have done much work on solvent-based polyurethanes with self-healable capacity. However, little research has been done on self-healable WPU through the combination of dynamic hydrogen bonds and boronic ester bonds. Also, the trend of environmental friendliness, avoiding the use of harmful volatile organic compounds (VOCs), and taking full advantage of waterborne polyurethane should be considered.

Herein, we introduce multiple hydrogen bonds and boronic ester bonds in the molecular structure of WPU to prepare a self-healable WPU elastomer. PTMG with flexible chain mobility for better self-healing, acted as the soft segment. IPDI was chosen as the hard segment with asymmetric, non-rigid and bulky structure, which can restrain the crystallization and facilitate the chain mobility.[5] DAP was selected as the chain extender and the primary amine group produced a urea group after chain extension, resulting in dihydrogen bonding, which may have a positive influence on the simultaneous improvement of mechanical performance and self-healing ability. BA was used as a dynamic crosslinker to form cross-linking points based on reversible boronic ester bonds in the polyurethane system, which not only improved the mechanical strength of the material, but also induced a reversible hydrolysis reaction, promoting the self-healing ability. Designing the recipe, the chain structure of the polymer was adjusted by controlling the ratio *n* (DAP/BA) of hard segments, the combination of multiple hydrogen bonds and boronic ester bonds, which could effectively satisfy the demands of good mechanical performance and desirable self-healing efficiency. Finally, we obtained waterborne polyurethane with good storage stability, water resistance, high strength and toughness, which also exhibited good self-healing ability by surface wetting and heating at 80 °C.

2 Experimental

2.1 Materials

Polytetrahydrofuran (PTMG, $M_n = 2000$ g mol^{-1}) was purchased from BASF (Germany). Dimethylolpropionic acid (DMPA, 98%) was purchased from Bide Pharmatech Ltd (China). Isophorone diisocyanate (IPDI), 2,6-diaminopyridine (DAP,98%), boric acid (BA,99.99%), and dibutyltin dilaurate (DBTDL) were provided by Aladdin (China). *N*,*N*-Dimethylformamide (DMF), acetone and triethylamine (TEA) were supplied by Sinopharm (China). DMF and acetone were dehydrated with molecular sieves over 72 h. Deionized (DI) water was self-made and used directly. PTMG was dried under vacuum at 110 °C for 2 h before use. DMPA was dehydrated at 130 °C for 60 min. The experiment was carried out under nitrogen protection.

2.2 Synthesis of waterborne polyurethanes (IP-DAP$_x$-BA$_y$-WPU)

Self-healable waterborne polyurethane emulsions with varying DAP and BA contents were synthesized *via* a typical polymerization method (Scheme 1), which were denoted as IP-DAP$_x$-BA$_y$-WPU, where *x* and *y* are the molar ratio of functional groups (DAP/BA), respectively, and their compositions are shown in Table 1. A typical procedure for the preparation of IP-DAP$_{40}$-BA$_{10}$-WPU is presented as follows. Firstly, PTMEG (48.00 g, 24.00 mmol) and IPDI (16.67 g, 75.00 mmol) were placed in a three-necked flask equipped with a mechanical stirrer at 70 °C under an N_2 atmosphere. Then, it was cooled to 60 °C, and DBTDL (0.14 g, 0.2 wt%) as the catalyst was injected into the flask. Then, it was heated to 80 °C, and after mixing for 1 h, DMPA (3.48 g, 26.00 mmol) was added and stirred for another 6 h to prepare the isocyanate-terminated pre-polymer. Subsequently, DAP (2.18 g, 19.98 mmol) dissolved in acetone (10.00 g) was injected and stirred for 2 h at 60 °C. Then, BA (0.21 g, 3.33 mmol) was introduced and reacted for about 2 h to consume the remaining isocyanates. Subsequently, the temperature was decreased to 30 °C and TEA (2.62 g, 26.00 mmol) was added for neutralization under stirring for 0.5 h. Then was emulsified with DI water at a stirring speed of 1500 rpm for 1 h. Finally, an appropriate amount of acetone was employed to adjust the viscosity during the process, which was removed by rotary evaporation and IP-DAP$_x$-BA$_y$-WPU was obtained.

2.3 Preparation of IP-DAP$_x$-BA$_y$-WPU films

The above-mentioned IP-DAP$_x$-BA$_y$-WPU emulsions were slowly poured into a polytetrafluorethylene mould (120 mm × 100 mm × 4 mm) and dried for 48 h at 25 °C and a further 72 h at 40 °C in a blast drying oven. When the film became a constant weight, it was thoroughly dried, and then taken out for further testing and characterization.

2.4 Instrumentation and characterization

The particle size and the distribution of the IP-DAP$_x$-BA$_y$-WPU emulsions were measured using a Zetasizer 3000HS at 25 °C.

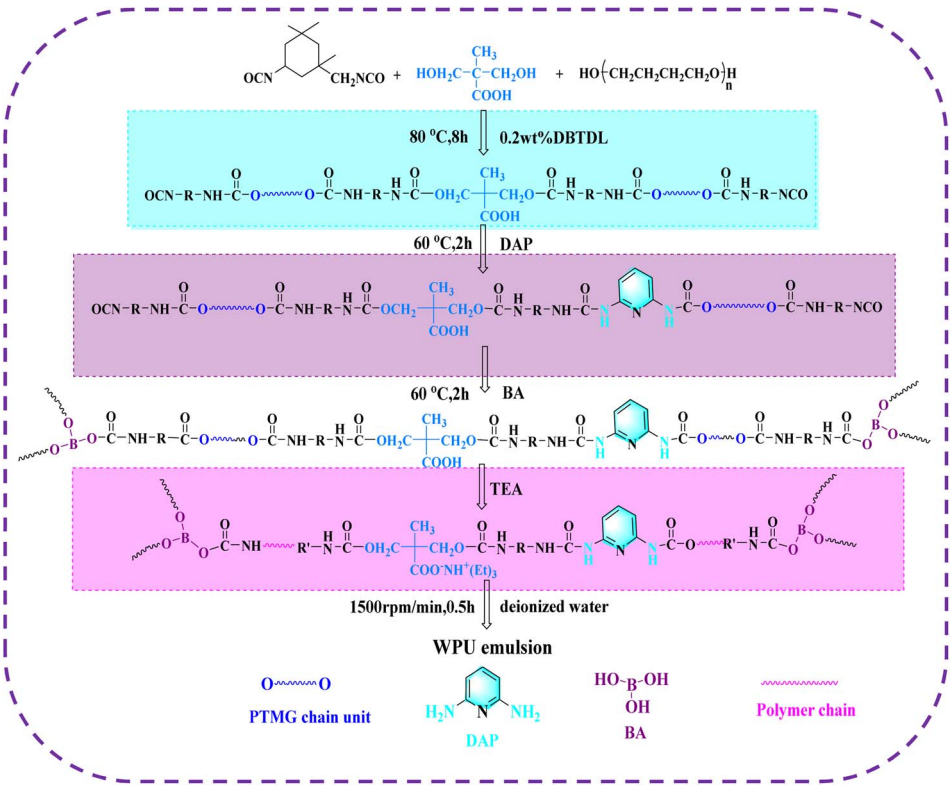

Scheme 1 Synthetic route for IP-DAP$_x$-BA$_y$-WPU emulsion.

Table 1 Composition of reactants for the synthesis of IP-DAP$_x$-BA$_y$-WPU (mmol)

Sample	IPDI	PTMG	DMPA	DAP	BA	TEA
IP-DAP$_{50}$-BA$_0$-WPU	75.00	24.00	26.00	25.00	0.00	26.00
IP-DAP$_{45}$-BA$_5$-WPU	75.00	24.00	26.00	22.50	1.67	26.00
IP-DAP$_{40}$-BA$_{10}$-WPU	75.00	24.00	26.00	19.98	3.33	26.00
IP-DAP$_{35}$-BA$_{15}$-WPU	75.00	24.00	26.00	17.50	5.00	26.00
IP-DAP$_{30}$-BA$_{20}$-WPU	75.00	24.00	26.00	15.00	6.67	26.00
IP-DAP$_{25}$-BA$_{25}$-WPU	75.00	24.00	26.00	12.50	8.33	26.00
IP-DAP$_0$-BA$_{50}$-WPU	75.00	24.00	26.00	0.00	16.67	26.00

The emulsions were diluted to about 0.01 wt% with distilled DI water before measurement. This measurement was repeated three times for each sample and the average value calculated.

The stability of the IP-DAP$_x$-BA$_y$-WPU emulsions (for 40 days) was determined using a centrifuge (TG16-WS, China). The emulsion was poured into a centrifuge tube and centrifuged at 3000 rpm for 0.5 h at ambient temperature.[48]

The water contact angle of the emulsions was determined by dropping them on a slide to form a film, and then the dried film was placed in a contact angle measuring instrument (JC2000C, Shanghai Zhongchen). Finally, the mean value of each sample test was taken five times and the droplet size of each test was kept consistent.

The water resistance of the WPU films was measured by water absorption, where they were cut into samples of about 2 cm × 2 cm × 0.2 cm and placed in DI water at room temperature for 24 h. Subsequently, the swollen film was taken out and the surface water was absorbed with filter paper. The water absorption percentage (WA) was calculated as follows:

$$\mathrm{WA} = \frac{M_0 - M_1}{M_0} \times 100\% \quad (1)$$

where M_0 and M_1 are the weight of the dry film and wet film, respectively.

Fourier transform infrared (FTIR) analysis (ATR-method) was carried out using a Nexus Spectrometer (Thermo Nicolet, USA) in the region of 4000 to 600 cm^{-1}.

Thermogravimetric analysis (TGA) was conducted on an STA449F3 thermal analyzer (Netzsch, Germany). The sample (5–10 mg) was heated from 25 °C to 800 °C at a rate of 10 °C min^{-1} under an N_2 atmosphere.

Differential scanning calorimetry (DSC) was performed using a DSC-Q2000 (TA Instrument) under an N_2 atmosphere from −80 °C to 80 °C at a ramping rate of 10 °C min^{-1}.

Dynamic mechanical analysis (DMA) was conducted on a DMA8000 instrument (PE, USA) in stretching mode with a rectangular size (20 × 5 × 1 mm). The heating rate was 3 °C min^{-1} and the frequency was 1 Hz. The temperature was increased from −150 °C to 150 °C during the process.

The whole mechanical performance was measured on a WDW-L02 universal testing machine. The dumbbell samples (75 mm × 4 mm), which were tested at a displacement rate of 50 mm min^{-1} at ambient temperature based on the GB/T13022-91 standard. Three replicates were measured for each sample at least.

Self-healing tests. Dumbbell-type samples were cut into two pieces using a sharp blade. Then, the parted films were carefully put together and placed in an oven for different durations.[22] The healing efficiency (η) was defined as the ratio of the stress or strain of the films after and before healing,[44,49] using the following equation:

$$\text{Healing efficiency } (\eta) = \frac{(\text{stress or strain of healed films})}{(\text{stress or strain of original films})} \times 100\% \quad (2)$$

A crack with created with a sharp blade to about 40% thickness in the IP-DAP$_x$-BA$_y$-WPU films and then heated for several hours in a heating stage at 80 °C with the surface wetting of water for 1 h. The healing effect of the scratches was directly observed using an optical microscope (UPT2001, China).

3 Results and discussion

3.1 Particle size and stability of IP-DAP$_x$-BA$_y$-WPU emulsions

The particle size and distribution are important physical parameters of the WPU emulsion, which are strongly associated with its appearance and dispersion stability. When water was added during the emulsification process, the polyurethane could form colloidal particles through phase inversion to achieve efficient dispersion in the aqueous phase. As shown in Fig. 1a, with an increase in boric acid content, the average particle size of the IP-DAP$_x$-BA$_y$-WPU emulsions increased gradually, which was 29.42 nm, 30.30 nm, 30.77 nm, 32.47 nm, 44.71 nm, 50.92 nm, respectively. Meanwhile, the distribution was uniform for all the samples, where the polydispersity (PDI) was in the range of 0.128 to 0.225. Usually, the particle size of a WPU emulsion is closely related to its chain stiffness, crystallinity, hydrophilic groups and cross-linking structure.[23] With an increase in the content of the boric acid cross-linking agent, the waterborne polyurethane molecular junction increased and the molecular chains had poor mobility, which could not assemble quickly to form latex particles in the emulsification, and thus the tightness of the formed latex particles became worse, and more boric acid also made it difficult to disperse in water, leading to larger particle sizes. Fig. 1b shows the color and appearance of the IP-DAP$_x$-BA$_y$-WPU emulsions in natural light, which were bright and atrovirens. As the particle size increased, the color deepened. Zeta potential is an important indicator to characterize the stability of the dispersion system, where a high absolute zeta potential value indicates that sufficient electrostatic repulsion exists on the surface of the WPU particles. The absolute value was in the range of 35 to 50 mV for all the IP-DAP$_x$-BA$_y$-WPU emulsions (Fig. 2b), which exhibited distinct values.[50] As shown in Fig. 1c, the IP-DAP$_x$-BA$_y$-WPU emulsions left for 40 days were centrifuged at 3000 rpm for 0.5 h, which all displayed good storage stability without evident precipitation or stratification.

3.2 Surface wettability and water resistance

As shown in Fig. 2a, with an increase in the amount of boric acid, the water contact angle (WCA) increased from 86.09° to 102.75°. Many polar hydrophilic groups dissociated on the surface of the IP-DAP$_{50}$-BA$_0$-WPU film containing only the chain extender, showing hydrophilicity. The crosslinking agent of BA will react with the hydrophilic groups to form cross-linking points inside, reduce the hydrophilic groups on the surface, and form a smooth film with lower surface energy, resulting in stronger hydrophobicity. When the amount of boric acid increased to a certain level, the residual hydrophilic polar groups on the surface increased, the WCA of the IP-DAP$_{25}$-BA$_{25}$-WPU film decreased to 93.65° (Fig. S1†).

Generally, the water absorption (WA) is influenced by the hydrophilic composition content and film surface structure. In our study, the water absorption of the specimens decreased with an increase in the BA/DAP molar ratio, which was only 7.9% of IP-DAP$_{35}$-BA$_{15}$-WPU. As the degree of cross-linking in the system gradually increased, the film surface formed was

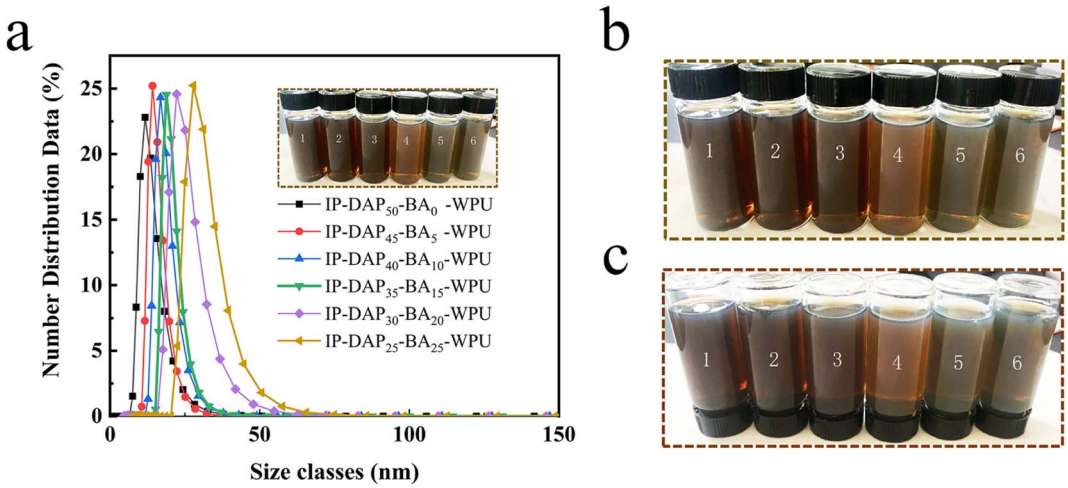

Fig. 1 (a) Particle size and distribution of the as-prepared WPU particles. Color and appearance of IP-DAP$_x$-BA$_y$-WPU emulsions (b) before and (c) after centrifugation in natural light.

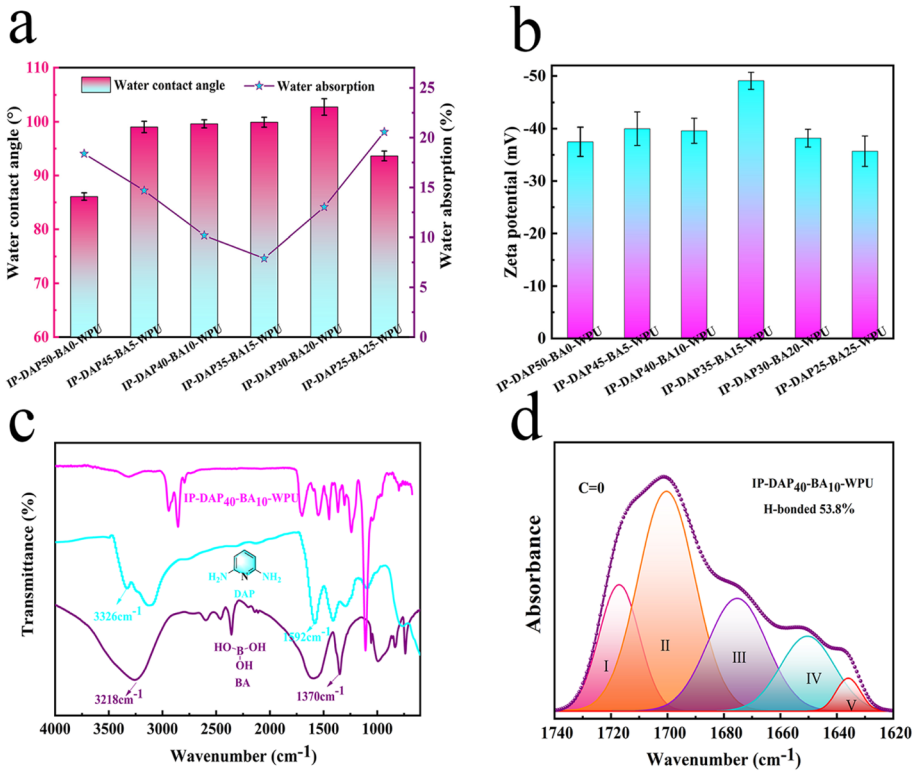

Fig. 2 (a) Water contact angle (WCA) and water absorption (WA) of different IP-DAP$_x$-BA$_y$-WPU samples. (b) Zeta potential values of different IP-DAP$_x$-BA$_y$-WPU emulsions. (c) FT-IR spectra of BA, DAP and IP-DAP$_{40}$-BA$_{10}$-WPU in the frequency range of 650–4000 cm^{-1}. (d) FTIR spectra of IP-DAP$_{40}$-BA$_{10}$-WPU in the C=O stretching vibration region.

denser, which left fewer polar groups on the surface and exhibited better water resistance. When the cross-linking density and the emulsion particle size were too large, more defects were left on the surface, making it easy for water to invade from these defects. The fractured surface morphology of the representative WPU films was further observed by SEM. As shown in Fig. S4,† with an increase in the content of BA cross-linking agent, the fractured surface gradually became rougher, which showed a typical ductile fracture.[10] The surface of IP-DAP$_{25}$-BA$_{25}$-WPU film was irregular and coarse, and thus the water absorption increased to 20.85%, which exhibited poor water resistance. In general, the synthetic polyurethane film had good water resistance, which overcame the disadvantage of poor water resistance of traditional waterborne polyurethane.

3.3 Chemical structure of IP-DAP$_x$-BA$_y$-WPU films

The chemical structure of the IP-DAP$_x$-BA$_y$-WPU samples was verified by FT-IR analysis. As depicted in Fig. 2b and S2,† the peaks at around 3320 cm^{-1} and 1549 cm^{-1} correspond to the –NH stretching and bending vibration of the urethane groups, respectively. The peaks at 2856 cm^{-1} and 2942 cm^{-1} correspond to the stretching vibration of –CH$_2$–.[22] The peak at 1110 cm^{-1} is assigned to the stretching vibration of C–O–C. The characteristic peaks at 1592 cm^{-1} and 1370 cm^{-1} are attributed to the C=N vibration mode of the free pyridine of 2,6-diaminopyridine (DAP) and B–O vibration mode of boric acid (BA), respectively, demonstrating that the DAP and BA moieties were introduced in the polymer backbones of IP-DAP$_x$-BA$_y$-WPU effectively.[51] Moreover, the disappearance of the typical –NCO peak at around 2260–2280 cm^{-1} indicates the completion of the reaction.[10,52]

The peaks at 1740 cm^{-1} to 1620 cm^{-1} are attributed to the different vibrations of C=O, which were further analyzed by peak fitting and differentiation, as shown in Fig. 2d. The C=O peaks were divided into five sub-peaks in the spectrum of IP-DAP$_{40}$-BA$_{10}$-WPU. The peak at 1714 cm^{-1} is attributed to the free C=O of urethane, and that at 1700 cm^{-1} attributed to the vibration of the ordered H-bond. The peak at 1673 cm^{-1} is assigned to the free C=O of urea and that at 1652 cm^{-1} to the disordered H-bond vibration of urea.[53] The vibration of the ordered H-bond in the urea appeared at 1637 cm^{-1}. These results indicate that the content of H-bonded C=O in the IP-DAP$_{40}$-BA$_{10}$-WPU was higher than 53.80%. Notably, the proportion of hydrogen bonds in IP-DAP$_{50}$-BA$_0$-WPU, IP-DAP$_{45}$-BA$_5$-WPU, IP-DAP$_{35}$-BA$_{15}$-WPU, IP-DAP$_{30}$-BA$_{20}$-WPU, and IP-DAP$_{25}$-BA$_{25}$-WPU are 46.82%, 51.62%, 43.79%, 39.75% and 31.25%, respectively (Fig. S3†). The formation of hydrogen bonds in C=O is mainly due urethane–urethane, urethane–urea, and urea–urea, in which the bonding energy of H-bond constructed by urea–urea is much higher than that with urethane–urethane.[32,45] Some of the boronic ester replaced the urea bond, where a bond with a lower bonding energy is easier to form, which may be more conducive to the formation of ordered hydrogen bonds. The presence of multiple hydrogen

bonds had a positive effect on promoting the mechanical performance and self-healing capacity.

3.4 Thermal properties of the IP-DAP$_x$-BA$_y$-WPU films

The thermal stability of polyurethane is critical for its practical application, which is closely connected with its rigid groups, cross-linked structure and crosslinking density.[54] The thermal degradation process was determined by TGA, as shown in Fig. 3a and b, where it can be observed that the representative IP-DAP$_{50}$-BA$_0$-WPU, IP-DAP$_{40}$-BA$_{10}$-WPU and IP-DAP$_{30}$-BA$_{20}$-WPU films all displayed two-stage decomposition steps. The initial weight loss of the film occurred in the first stage at about 230–320 °C, which is attributed to the decomposition of the hard segment. The decomposition temperature in the second stage was 360–438 °C, which is attributed to the degradation of the soft segments. In addition, it was observed that the mass loss of 10% occurred 297.36 °C, 300.62 °C and 303.18 °C, while the mass loss of 50% occurred at 405.19 °C, 407.12 °C and 410.34 °C for the IP-DAP$_{50}$-BA$_0$-WPU, IP-DAP$_{40}$-BA$_{10}$-WPU and IP-DAP$_{30}$-BA$_{20}$-WPU samples, respectively. With an increase in the cross-linking density, the thermal decomposition temperature increased slightly, but the effect was not significant, where all the samples exhibited good thermal stability below 200 °C.

According to the DSC analysis, as shown in Fig. 3c, the glass transition temperature (T_g) of WPU was not distinct in the DSC curve, and thus a DMA test was further employed to determine it visually. As shown in Fig. 3d, the measured glass transition temperatures were −54.47 °C, −55.15 °C and −53.46 °C, respectively. Adjusting the ratio n (DAP/BA) of hard segments, the composition of hydrogen bonds to boronic ester bonds in the polymer chain further changed, but the three films had the same ratio of soft segments and hard segments, which had little effect on T_g. This further shows that the samples have good chain mobility, which will have a positive impact on the self-healing process.

3.5 Mechanical properties of IP-DAP$_x$-BA$_y$-WPU films

Mechanical properties are important parameters to measure for practical applications, which are affected by various factors such as intermolecular forces, physicochemical cross-linking, and rigidity in the molecular chains.[27] In this work, the molecular chain structure was designed by adjusting the ratio n (DAP/BA) of hard segments, aiming to obtain the desired mechanical robustness and chain mobility synchronously. As shown in Fig. 4a and b, the tensile stress, elongation and toughness were 18.89 ± 0.92 MPa, 898.16 ± 46.32% and 54.82 ±

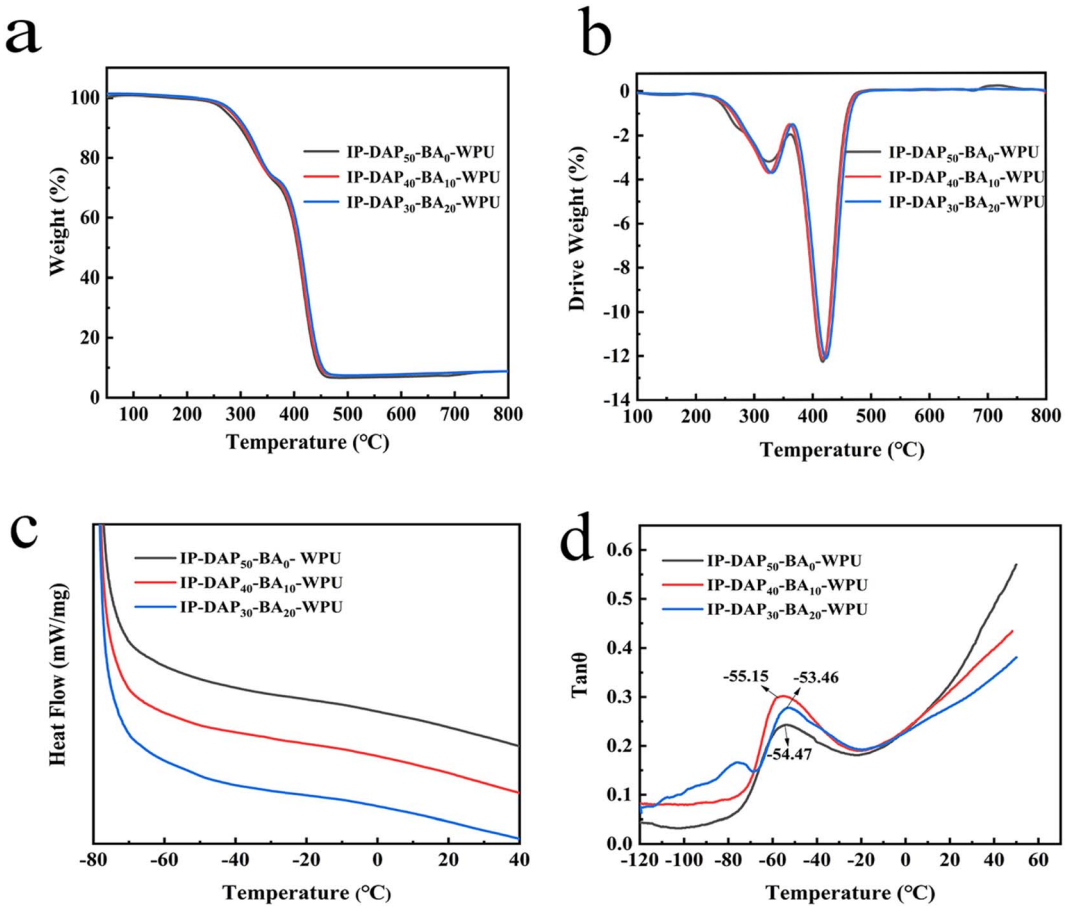

Fig. 3 (a) TGA curves, (b) DTG curves, (c) DSC curves, and (d) loss factor (tan θ) of the representative IP-DAP$_{50}$-BA$_0$-WPU, IP-DAP$_{40}$-BA$_{10}$-WPU and IP-DAP$_{30}$-BA$_{20}$-WPU samples.

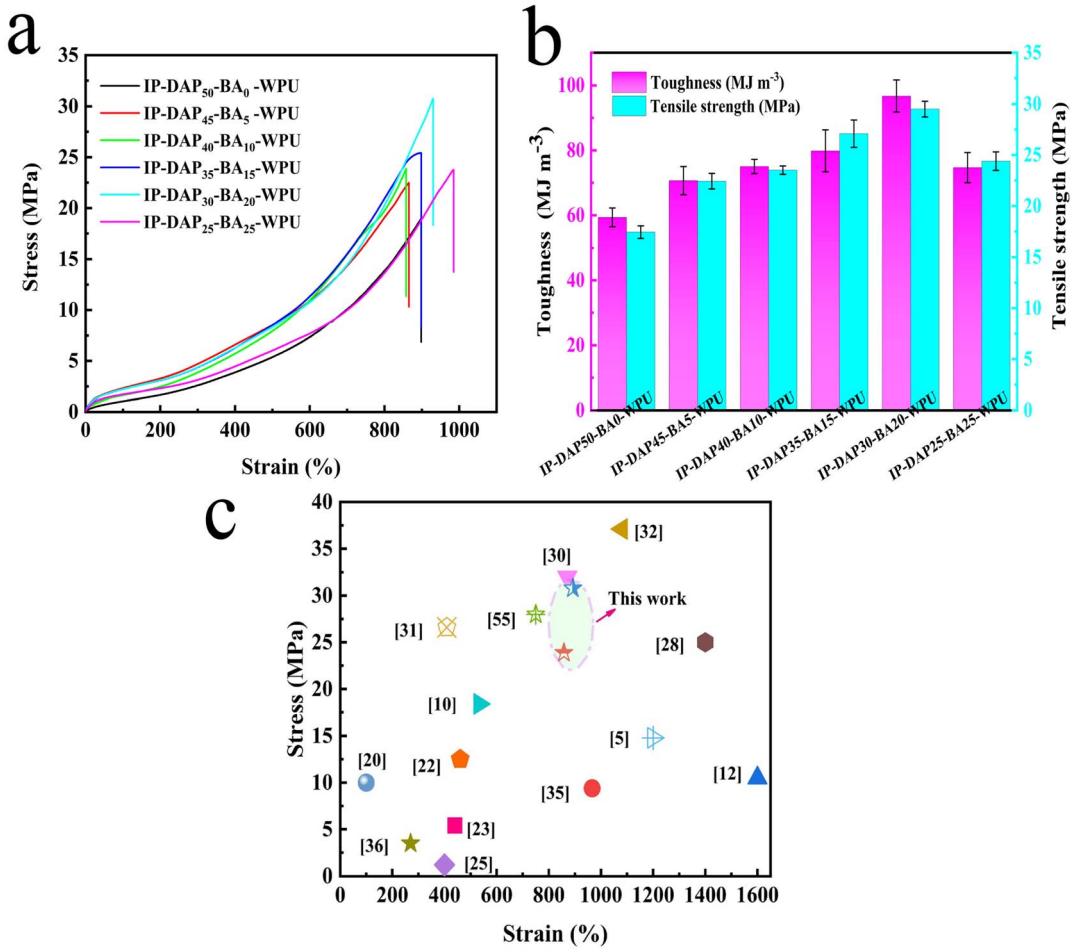

Fig. 4 (a) Stress–strain curves. (b) Tensile strength and toughness of different IP-DAP$_x$-BA$_y$-WPU films. (c) Mechanical performance of the representative IP-DAP$_{40}$-BA$_{10}$-WPU and IP-DAP$_{30}$-BA$_{20}$-WPU films in this work compared with those of other studies.

1.93 MJ m^{-3} for the pure IP-DAP$_{50}$-BA$_0$-WPU film, respectively. With an increase in the boric acid content, the tensile stress and toughness gradually increased, while the elongation remained basically unchanged (Table S2†). Particularly, the IP-DAP$_{30}$-BA$_{20}$-WPU film exhibited excellent mechanical properties, which were 30.78 ± 1.56 MPa, 930.12 ± 48.54%, 92.74 ± 2.42 MJ m^{-3}, respectively. In the case of self-healable waterborne polyurethane, there are few similar high strength and toughness elastomers in other studies. The pristine IP-DAP$_{50}$-BA$_0$-WPU elastomer only contained urea doublet hydrogen bonding and urethane singlet hydrogen bonding in its hard segment domains, which serve as physical cross-linking junctions. However, the ratio of n (DAP/BA) could promote the degree of phase separation, the dynamic boronic ester bond could enhance intermolecular force as a point of cross-linking, and also served as sacrificial bonds with hydrogen bonding to increase the hidden length of the folded polymer chain, thus enhancing the mechanical properties.[12] Meanwhile, excessive cross-linking will generate stress concentration, which destroys the specimen before it can disperse more stress, resulting in mechanical deficiency.[26] Undesirably, when using pure boric acid, there were many film-forming defects in IP-DAP$_0$-BA$_{50}$-WPU, which exhibited terrible mechanical properties and poor self-healing ability (Table S2†). It failed to yield further application value. Thus, based on the above-mentioned results, tuning the moderate degree of cross-linking and components of the hard segments could promote the mechanical properties of self-healable WPU elastomers efficiently.

3.6 Cyclic tensile tests of IP-DAP$_x$-BA$_y$-WPU films

The multiple dynamic hydrogen bonds and covalent boronic ester bonds in the films were expected to endow them with high toughness and good elasticity, respectively. Thus, to further assess their performance, we conducted a cyclic tensile test. Taking the IP-DAP$_{30}$-BA$_{20}$-WPU film as an example, there was no waiting period in the continuous cyclic tensile test (Fig. 5a), which involved two successive loadings. Following the first small-strain (100%) stretching cycle, there was an entropic drive for the covalent network and the unbroken reversible bonds (hydrogen and boronic ester bonds) to return the network almost to its pristine status. Under sequential cyclic larger strain (≥200%), large hysteresis loops could be seen clearly owing to the energy dissipation resulting from the reformation of broken dynamic bonds at new sites during stretching, but the

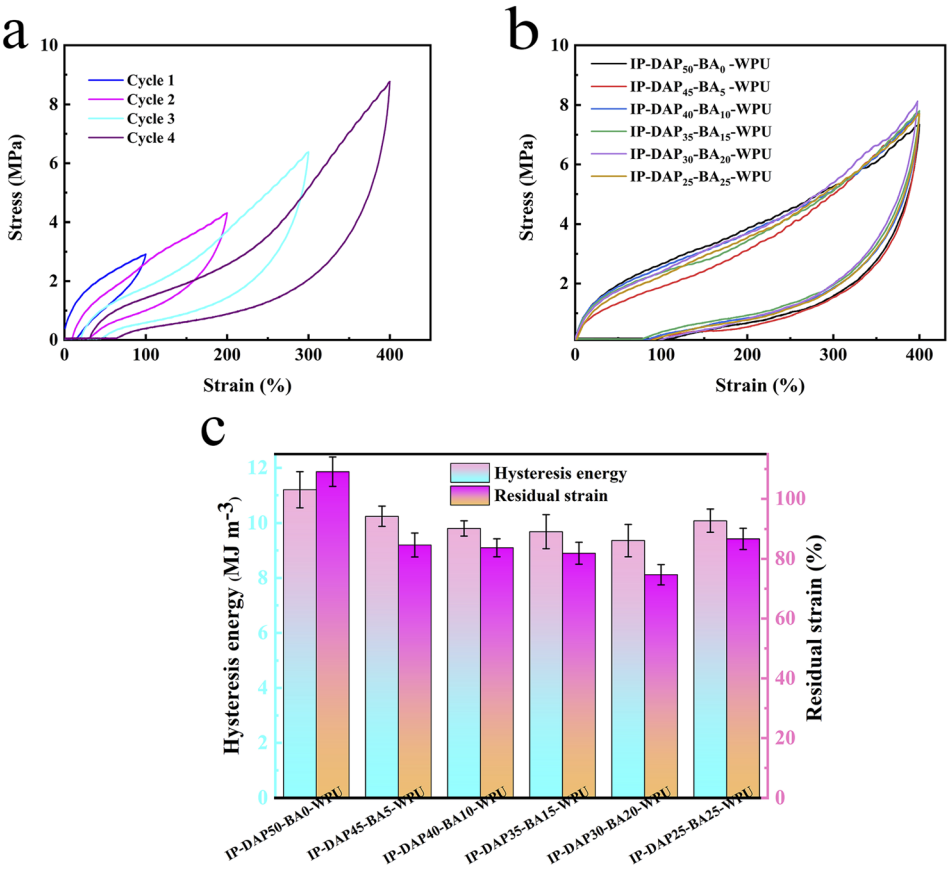

Fig. 5 (a) Sequential cyclic tensile curves of the IP-DAP$_{30}$-BA$_{20}$-WPU film at different strains without waiting time. (b) Cyclic tensile curves of IP-DAP$_x$-BA$_y$-WPU films with a maximum strain of 400%. (c) Residual strain and hysteresis energy of IP-DAP$_x$-BA$_y$-WPU films during the cyclic tensile processes.

residual strain remained low. This revealed that IP-DAP$_{30}$-BA$_{20}$-WPU had good elasticity with a strain of 200%, making it suitable for many practical applications.

To further reveal how the hydrogen bonds and boronic ester bonds affected the mechanical properties of the films, cyclic tensile tests were carried out. Fig. 5b and c exhibit the loading–unloading cycle curve at a fixed strain of 400% and comparison with the hysteresis loop, respectively. The IP-DAP$_{50}$-BA$_0$-WPU film had the maximum area hysteresis loop area (mechanical hysteresis) compared to the other elastomers. The mechanical hysteresis resulted in the delayed recovery of its configuration and conformation caused by the friction between the polymer chains. In the case of the IP-DAP$_{50}$-BA$_0$-WPU elastomer, the hydrogen bonding between the urea group, urethane group and pyridine was the main interchain force that restricted the polymer segment from reforming. For the elastomer with boronic ester bonds, the presence of boronic ester bonds significantly interfered with the formation of hydrogen bonds between the urea groups, and the cross-linking point limited the slip of the molecular chain as well, which was beneficial for the recovery of the polymer chain configuration and conformation, resulting in a slight lag curve. In conclusion, the high elasticity of the elastomers could be significantly improved by adjusting the composition of hard segments reasonably.

3.7 Self-healing properties of IP-DAP$_x$-BA$_y$-WPU films

The self-healing performance was firstly studied at 60 °C for different healing times. As shown in Fig. 6, it can be observed that the strength of the representative samples healed for 36 h of IP-DAP$_{50}$-BA$_0$-WPU, IP-DAP$_{40}$-BA$_{10}$-WPU and IP-DAP$_{30}$-BA$_{20}$-WPU was 5.63 MPa, 9.41 MPa, 9.46 MPa, respectively. Although IP-DAP$_{40}$-BA$_{10}$-WPU exhibited the higher healing efficiency of elongation of 72.30%, its strength was undesirable. The motility of the molecular chains was not strong at the lower temperature was 60 °C, and thus higher activation energy would be required. In our study, the self-healing systems *via* multi-dynamic interactions needed to be exposed to higher external stimulus.

To further investigate the self-healing behavior of the IP-DAP$_x$-BA$_y$-WPU films, their healing efficiency was studied at 80 °C by the tensile test taking the IP-DAP$_{50}$-BA$_0$-WPU, IP-DAP$_{40}$-BA$_{10}$-WPU and IP-DAP$_{30}$-BA$_{20}$-WPU films as examples. As depicted in Fig. 7(a–c) and (e), after undergoing thermal repair at 80 °C for 40 h, the strength was only 7.32 MPa for the IP-DAP$_{50}$-BA$_0$-WPU film, which exhibited low self-healing efficiency of 38.61%. By contrast, the IP-DAP$_{40}$-BA$_{10}$-WPU film exhibited stress of 21.26 MPa and strain of 679.52%, which were 89.07% and 79.02% self-healing efficiency, respectively. Compared with the pure IP-DAP$_{50}$-BA$_0$-WPU film, its self-repairing ability had been greatly improved. Therefore, the

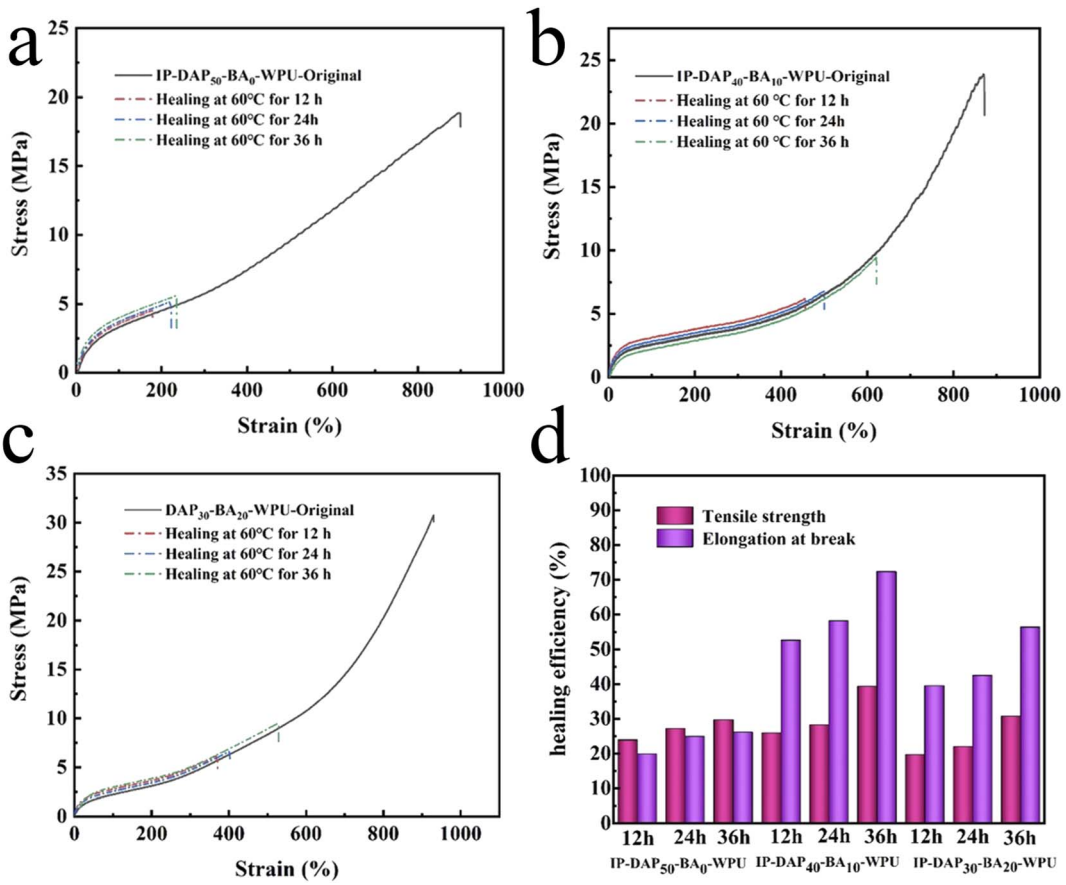

Fig. 6 Original and self-healed tensile stress–strain curves (a–c) and self-healing efficiency (d) of IP-DAP_{50}-BA_0-WPU, IP-DAP_{40}-BA_{10}-WPU and IP-DAP_{30}-BA_{20}-WPU films after healing at 60 °C for 12 h, 24 h, and 36 h.

existence of a too high DAP content with the structural rigidity of its hard segments and lower hydrogen bonding will weaken the mobility of the segments, which is adverse to the healing process. The combination of dynamic reversible non-covalent bonds (multiple hydrogen bonds) and covalent bonds (boronic ester bond) was more favorable for self-healing. The IP-DAP_{30}-BA_{20}-WPU film had stress of 17.34 MPa and strain of 627.76%, which were 56.33% and 69.85% of the self-healing efficiency, respectively. The higher content of hard segments with boric acid content vastly enhanced its strength, but sharply weakened its chain mobility, giving rise to reduced self-healable capacity. Undesirably, the IP-DAP_{25}-BA_{25}-WPU film had stress of 8.73 MPa and strain of 422.70%, which were 36.74% and 55.12% of the self-healing efficiency, respectively (Table S3†). The research on self-healing materials is focused on how to achieve a satisfactory balance between mechanical performance and healing capacity. Appropriate dynamic crosslinking points not only can strengthen and toughen materials, but also ensure better chain mobility, aiming to effectively repair them under mild conditions. However, too many cross-linking points constrain the molecular chain movement, requiring a higher energy to activate the chain segment and mobility, thus showing poor repairing ability. Consequently, the healing efficiency can be significantly improved by reasonably adjusting the composition of the hard segments.

More interestingly, the self-healing behaviors of the IP-DAP_x-BA_y-WPU films was significantly influenced by water. Specifically, a cut section was soaked in water for 30 s, and then placed in an oven at 80 °C. At regular intervals, water was dripped on the contact surface with a dropper until the healing time was almost over, and then the surface was dried with filter paper. The results show that the healing efficiency improved dramatically with the support of water. It was observed that the typical IP-DAP_{40}-BA_{10}-WPU film healed for 36 h with the aid of water could be easily stretched to several times of its original length, as presented in Fig. 8b. Furthermore, the IP-DAP_{40}-BA_{10}-WPU film could hold a weight of 2.25 kg and also showed good self-recovery ability, as shown in Fig. 8c. Fig. 7d and f depicted the representative stress–strain curves and healing efficiency of the IP-DAP_{40}-BA_{10}-WPU film, which recovered for diverse lengths of time without water or with the aid of water, respectively. The IP-DAP_{40}-BA_{10}-WPU film healed at 80 °C for 36 h with the support of water, which exhibited the stress of 21.67 MPa and strain of 787.29%, which were 90.74% and 91.29% healing efficiency, respectively. Driven by both water and heat, they not only shortened the repair time, but also improved the healing efficiency (Table S4†).

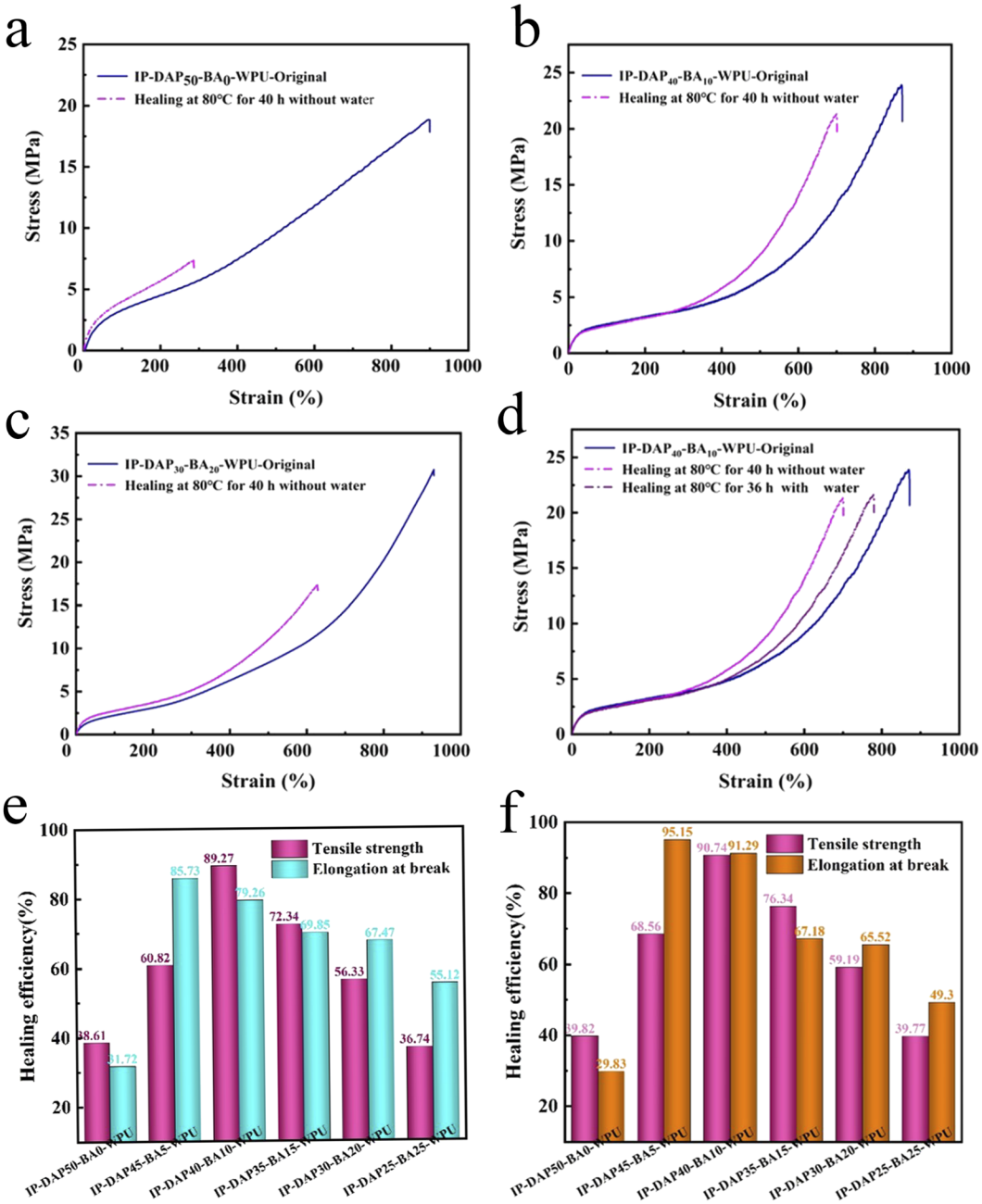

Fig. 7 Original and self-healed tensile stress–strain curves (a–c) of IP-DAP$_x$-BA$_y$-WPU films after healing at 80 °C for 40 h without water. (d) Representative original and self-healed tensile stress–strain curves of IP-DAP$_{40}$-BA$_{10}$-WPU films under different conditions. (e) Self-healing efficiency of IP-DAP$_x$-BA$_y$-WPU films healed at 80 °C for 40 h without water and (f) healed at 80 °C for 36 h with the aid of water.

The self-healing ability of the film could be intuitively evaluated through the recovery of its surface scratches by heating on a hot plate at 80 °C with surface wetting for 1 h. A polarizing microscope was employed to record the entire healing process. As shown in Fig. 8a, the IP-DAP$_{50}$-BA$_0$-WPU film retained a deep, wide scratch. With an increase in the amount of boric acid, which replaced pyridine in the hard segments, the scratches on its surface became lighter and its color became weaker. It was clear that the IP-DAP$_{40}$-BA$_{10}$-WPU film exhibited the most desirable thermal self-healing capacity, where the contact surface exhibited no obvious fracture trace. When the cross-linking density was too large, the surface scratches became deeper and the healing effect worsened. In contrast, the scratch in the IP-DAP$_{25}$-BA$_{25}$-WPU film was visible and barely healed, which displayed poor self-healing ability.

3.8 Self-healing mechanism

The desirable mechanical strength and self-healable capacity of the IP-DAP$_x$-BA$_y$-WPU film should be attributed to the multiple dynamic networks, as shown in Fig. 9, which involved three categories of dynamic non-covalent bonds (hydrogen bonds of urethane/urea and hydrogen-bonded pyridine) and one

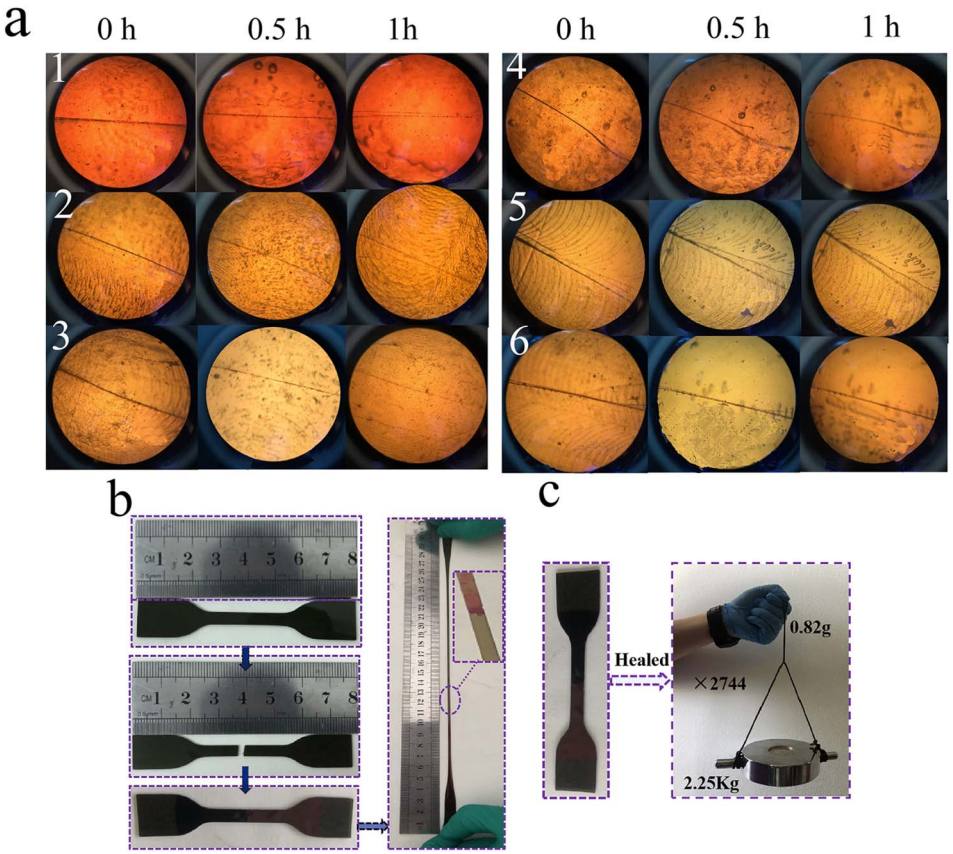

Fig. 8 (a) Crack healing photos of IP-DAP$_x$-BA$_y$-WPU film at 80 °C with the surface wetting of water for 1 h observed using a 200× optical microscope: 1-IP-DAP$_{50}$-BA$_0$-WPU, 2-IP-DAP$_{45}$-BA$_5$-WPU, 3-IP-DAP$_{40}$-BA$_{10}$-WPU, 4-IP-DAP$_{35}$-BA$_{15}$-WPU, 5-IP-DAP$_{30}$-BA$_{20}$-WPU, and 6-IP-DAP$_{25}$-BA$_{25}$-WPU. (b) Stretching picture of IP-DAP$_{40}$-BA$_{10}$-WPU film (75 mm × 4 mm × 1 mm) healed for 36 h at 80 °C with water and (c) subjected to a 2.25 kg weight lifting test.

reversible covalent bond (boronic ester bond). The primary amine group of 2,6-diaminopyridine produced a urea group after chain extension, resulting in dihydrogen bonding, where its cohesive energy was higher than that of the urethane group, which was conducive to enhancing the mechanical performance of the elastomer. However, the pure-IP-DAP$_{50}$-BA$_0$-WPU

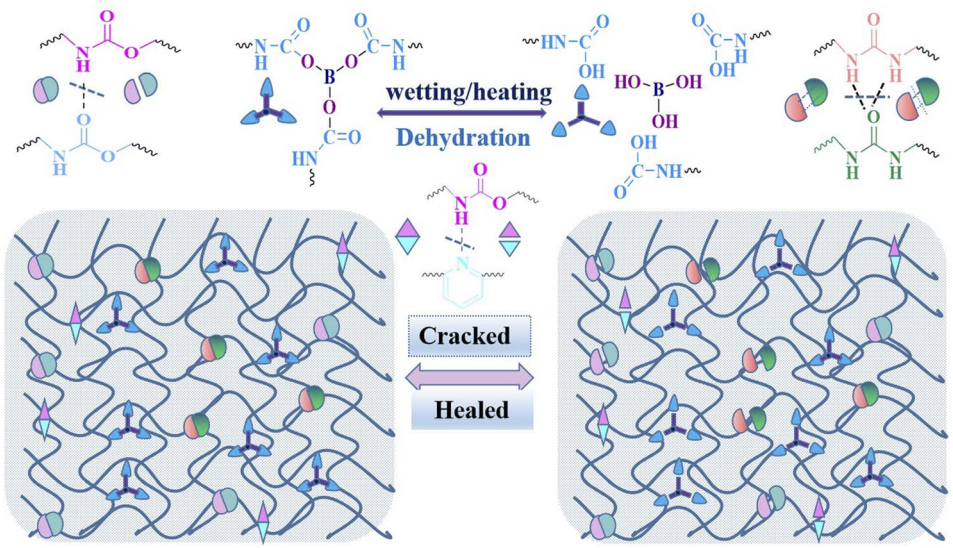

Fig. 9 Schematic diagram of self-healable mechanism of IP-DAP$_x$-BA$_y$-WPU film.

film exhibited low self-healable capacity, which just relies on dynamic hydrogen bonds. Introducing new active cross-linking agents and adjusting the ratio n (DAP/BA) of hard segments could effectively promote the mechanical properties and not compromise the self-healing ability. The IP-DAP_{40}-BA_{10}-WPU film had strength of 23.88 ± 0.69 MPa, breaking strain of 857.98 ± 26.88% and toughness of 73.91 ± 1.29 MJ m^{-3}, which showed a good level compared to other studies on waterborne polyurethane. Predominantly, driven by both water and heat, it showed excellent self-healing efficiency of above 90.0%. When water was dripped on the damaged surface, the boronic esters were hydrolyzed into boronic acids. Meanwhile, the hydrogen bonds of urethane and hydrogen-bonded pyridine were also partially broken.[12,18,55] The dissociation of the boronic ester bonds and hydrogen bonds enhanced the chain mobility dramatically. When the two sides of the fractured sample were contacted, the cross-linking structure at the sample section was undocked under the joint action of heating and water, and the molecular chains at both sides of the fracture surface could move, diffuse and tangle freely, gradually completing the section repair.

4 Conclusions

In summary, a series of environmentally friendly waterborne polyurethanes (IP-DAP_x-BA_y-WPU) with desirable mechanical strength and self-healable capacity at mild temperature were fabricated by employing 2,6-diaminopyridine (DAP) as a dynamic chain extender and boric acid (BA) as a dynamic cross-linking agent, which contained multiple hydrogen bonds and boronic ester bonds in their polymer backbone. The prepared waterborne polyurethanes (IP-DAP_x-BA_y-WPU) exhibited excellent storage stability, water resistance and thermal stability. Varying the ratio n (DAP/BA) of hard segments and adjusting the chain structure of the polymer could effectively overcome the contradiction between mechanical strength and healing efficiency. IP-DAP_{30}-BA_{20}-WPU exhibited good mechanical properties, such as tensile stress (30.78 ± 1.56 MPa), stretchability (930.12 ± 48.54%) and toughness (92.74 ± 2.42 MJ m^{-3}), respectively. It was found that a wide scratch on IP-DAP_{40}-BA_{10}-WPU film healed at 80 °C with the support of water, and after 1 h was almost no visible fracture trace. Driven by both water and heat, they shortened the healing time and improved the healing efficiency. The IP-DAP_{40}-BA_{10}-WPU film was cut in the middle and healed at 80 °C for 36 h with the aid of water, exhibiting desirable self-healing properties and the healing efficiency of tensile strength and breaking elongation were above 90.0%, which could hold a weight of 2.25 kg easily. Thus, it shows broad application prospects in flexible electronics, smart coatings and adhesives.

Author contributions

Qingsong Shi: methodology, formal analysis, writing – original draft. Weilin Wu: methodology, data curation, validation. Bing Yu: supervision, validation, Mengqing Ren: investigation. Lili Wu: funding acquisition, resources, writing – review & editing. Chaocan Zhang: project administration.

Conflicts of interest

The authors report no declarations of interest.

Acknowledgements

This research was supported by Guangdong Pustar Adhesives & Sealants Co. Ltd and Major Science and Technology Project in Zhongshan City, Guangdong Province (2020AG028).

References

1 Z. Wang, X. Lu, S. Sun, C. Yu and H. Xia, *J. Mater. Chem. B*, 2019, **31**, 4876–4926.
2 S. H. Cho, S. R. White and P. V. Braun, *Adv. Mater.*, 2009, **21**, 645–649.
3 C. C. Su and J. S. Chen, *Key Eng. Mater.*, 2017, **727**, 482–489.
4 M. Wang, J. Zhou, X. Jiang, Y. Sheng and X. Lu, *Eur. Polym. J.*, 2021, **146**, 110257.
5 L. Zhang, Z. Liu, X. Wu, Q. Guan, S. Chen, L. Sun, Y. Guo, S. Wang, J. Song and E. M. Jeffries, *Adv. Mater.*, 2019, **31**, 1901402.
6 Y. Fang, J. Xu, F. Gao, X. Du, Z. Du, X. Cheng and H. Wang, *Composites, Part B*, 2021, **219**, 108965.
7 H. Wang, J. Xu, X. Du, Z. Du, X. Cheng and H. Wang, *Composites, Part B*, 2021, **225**, 109273.
8 X. Wen, J. Xu, H. Wang, Z. Du, S. Wang and X. Cheng, *Polym. Eng. Sci.*, 2022, **62**, 3132–3143.
9 Z. Shi, J. Kang and L. Zhang, *ACS Appl. Mater. Interfaces*, 2020, **12**, 23484–23493.
10 L. Yang, B. Zla, B. Zza, B. Jwa, B. Lsa and B. Txa, *Prog. Org. Coat.*, 2021, **153**, 106153.
11 W. Zou, J. Dong, Y. Luo, Q. Zhao and T. Xie, *Adv. Mater.*, 2017, **29**, 1606100.
12 K. Song, W. Ye, X. Gao, H. Fang, Y. Zhang, Q. Zhang and X. Li, *Mater. Horiz.*, 2021, **8**, 216–223.
13 X. Chen, Q. Zhong, C. Cui, L. Ma, S. Liu, Q. Zhang, Y. Wu, L. An, Y. Cheng, S. Ye, X. Chen, Z. Dong, Q. Chen and Y. Zhang, *ACS Appl. Mater. Interfaces*, 2020, **12**, 30847–30855.
14 J. Zhou, H. Liu, Y. Sun, C. Wang and K. Chen, *Adv. Funct. Mater.*, 2021, **31**, 2011133.
15 P. F. Cao, B. Li, T. Hong, J. Townsend, Z. Qiang, K. Xing, K. D. Vogiatzis, Y. Wang, J. Mays and A. P. Sokolov, *Adv. Funct. Mater.*, 2018, **28**, 1800741.
16 B. Xu, F. Han, X. Pei, S. Zhang and J. Zhao, *Ind. Eng. Chem. Res.*, 2021, **60**, 11095–11105.
17 S. Yang, X. Du, S. Deng, J. Qiu and H. Wang, *Chem. Eng. J.*, 2020, **398**, 125654.
18 J. J. Cash, T. Kubo, A. P. Bapat and B. S. Sumerlin, *Macromolecules*, 2015, **48**, 2098–2106.
19 O. R. Cromwell, J. Chung and Z. Guan, *J. Am. Chem. Soc.*, 2015, **137**, 6492–6495.
20 J. C. Lai, J. F. Mei, X. Y. Jia, C. H. Li, X. Z. You and Z. Bao, *Adv. Mater.*, 2016, **28**, 8277–8282.

21 C. Yi, Z. Tang, X. Zhang, Y. Liu, S. Wu and B. Guo, *ACS Appl. Mater. Interfaces*, 2018, **10**, 24224–24231.
22 J. Rong, J. Zhong, W. Yan, M. Liu, Y. Zhang, Y. Qiao, C. Fu, F. Gao, L. Shen and H. He, *Polymer*, 2021, **221**, 12365.
23 T. Wan and D. Chen, *J. Mater. Sci.*, 2016, **52**, 197–207.
24 X. Wu, J. Li, G. Li, L. Ling, G. Zhang, R. Sun and C.-P. Wong, *J. Appl. Polym. Sci.*, 2018, **135**, 46532.
25 S. Ji, W. Cao, Y. Yu and H. Xu, *Adv. Mater.*, 2015, **27**, 7740–7745.
26 J. Hu, R. Yang, L. Zhang, Y. Chen, X. Sheng and X. Zhang, *Polymer*, 2021, **22**, 123674.
27 W. Fan, Y. Jin and L. Shi, *Polym. Chem.*, 2020, **11**, 5463–5474.
28 J. Hu, R. Mo, X. Jiang, X. Sheng and X. Zhang, *Polymer*, 2019, **183**, 121912.
29 Z. Liu, L. Zhang, Q. Guan, Y. Guo, J. Lou, D. Lei, S. Wang, S. Chen, L. Sun, H. Xuan, E. M. Jeffries, C. He, F. L. Qing and Z. You, *Adv. Funct. Mater.*, 2019, **29**, 1901058.
30 H. Peng, X. Du, X. Cheng, H. Wang and Z. Du, *Prog. Org. Coat.*, 2021, **151**, 106081.
31 N. Sun, M. Di and Y. Liu, *Int. J. Biol. Macromol.*, 2021, **184**, 1–8.
32 J. Xie, L. Fan, D. Yao, F. Su, Z. Mu and Y. Zheng, *Mater. Today Chem.*, 2022, **23**, 100708.
33 G. Gai, L. Liu, C. H. Li, R. K. Bose, D. Li, N. Guo and B. Kong, *ChemPlusChem*, 2019, **84**, 432–440.
34 C. H. Li and J. L. Zuo, *Adv. Mater.*, 2020, **32**, 1903762.
35 Y.-h. Li, W.-j. Guo, W.-j. Li, X. Liu, H. Zhu, J.-p. Zhang, X.-j. Liu, L.-h. Wei and A.-l. Sun, *Chem. Eng. J.*, 2020, **393**, 124583.
36 J. Liu, Y. Liu, Y. Wang, J. Zhu, J. Yu and Z. Hu, *Mater. Today Commun.*, 2017, **13**, 282–289.
37 Z. Wang, C. Xie, C. Yu, G. Fei, Z. Wang and H. Xia, *Macromol. Rapid Commun.*, 2018, **39**, 1700678.
38 X. Li, R. Yu, Y. He, Y. Zhang, X. Yang, X. Zhao and W. Huang, *ACS Macro Lett.*, 2019, **8**, 1511–1516.
39 X. Wang, D. Liang and B. Cheng, *Compos. Sci. Technol.*, 2020, **193**, 108127.
40 J. Liu, C. Tan, Z. Yu, N. Li, C. Abell and O. A. Scherman, *Adv. Mater.*, 2017, **27**, 1605325.
41 X. L. Wu, X. M. Zhang, S. Y. Huang, W. N. Zhou and Z. C. Wang, *Acta Crystallogr., Sect. C: Cryst. Struct. Commun.*, 2013, **69**, 730–733.
42 J. F. Mei, X. Y. Jia, J. C. Lai, Y. Sun, C. H. Li, J. H. Wu, Y. Cao, X. Z. You and Z. Bao, *Macromol. Rapid Commun.*, 2016, **37**, 1667–1675.
43 S. Cao, S. Li, M. Li, L. Xu, H. Ding, J. Xia, M. Zhang and K. Huang, *Polym. J.*, 2017, **49**, 775–781.
44 Q. Zhang, S. Niu, L. Wang, J. Lopez, S. Chen, Y. Cai, R. Du, Y. Liu and Z. Bao, *Adv. Mater.*, 2018, **30**, 1801435.
45 L. Xia, H. Tu, W. Zeng, X. Yang, M. Zhou and L. Li, *J. Mater. Chem. A*, 2022, **10**, 4344–4354.
46 A. P. Bapat, D. Roy, J. G. Ray, D. A. Savin and B. S. Sumerlin, *J. Am. Chem. Soc.*, 2011, **133**, 19832.
47 J. Liu, C. S. Y. Tan, Z. Yu, N. Li, C. Abell and O. A. Scherman, *Adv. Mater.*, 2017, **29**, 1605325.
48 H. Liang, L. Liu, J. Lu, M. Xhen and C. Zhang, *Ind. Crops Prod.*, 2018, **117**, 169–178.
49 R. H. Aguirresarobe, S. Nevejans, B. Reck, L. Irusta, H. Sardon, J. M. Asua and N. Ballard, *Prog. Polym. Sci.*, 2021, **114**, 101362.
50 A. Fs, B. Hza, A. Jq, A. Jw, A. Xz, B. C. Yang and Y. A. Peng, *Appl. Surf. Sci.*, 2021, **573**, 151526.
51 A. Sun, W. Guo, J. Zhang, W. Li, X. Liu, H. Zhu, Y. Li and L. Wei, *Polymers*, 2019, **11**, 1320.
52 L. Lyu, D. Li, Y. Chen, Y. Tian and J. Pei, *Constr. Build. Mater.*, 2021, **293**, 123480.
53 D. Fu, X. Yang, L. Guo and Y. Wang, *J. Mater. Chem. A*, 2022, **10**, 10139–10149.
54 T. Ghosh and N. Karak, *ACS Sustainable Chem. Eng.*, 2018, **6**, 4370–4381.
55 R. Liang, H. Zhang, Y. Wang, J. Ye, L. Guo, L. He, X. Li, T. Qiu and X. Tuo, *Chem. Eng. J.*, 2022, **442**, 136204.